SAR Image Segmentation Based on Fuzzy Region Competition Method and Gamma Model

Cunliang Liu[a,b]
[a]College of Information Science & Engineering, Shandong University of Science & Technology, Qingdao, China
Email: clliuqdu@gmail.com

Yongguo Zheng[a], Zhenkuan Pan[b], Jinming Duan[b] and Guodong Wang[b]
[b]College of Information Engineering, Qingdao University, Qingdao, China
Email: zhengyg206@163.com, zkpan@qdu.edu.cn, duanmujinming@126.com, doctorwgd@gmail.com

***Abstract*—In this paper, we present a novel variational framework for multiphase synthetic aperture radar (SAR) image segmentation based on the fuzzy region competition method. A new energy functional is proposed to integrate the Gamma model and the edge detector based on the ratio of exponentially weighted averages (ROEWA) operator within the optimization process. To solve the optimization problem efficiently, the functional is firstly modified to be convex and differentiable by using the fuzzy membership functions. And then the constrained optimization problem is converted to an unconstrained one by using the variable splitting techniques and the augmented Lagrangian method (ALM). Finally the energy is minimized with an alternative iterative minimization algorithm. The effectiveness of our proposed algorithm is validated by experiments on both synthetic and real SAR images.**

***Index Terms*—SAR image, segmentation, ROEWA, fuzzy membership functions, augmented Lagrangian method**

I. Introduction

The segmentation of synthetic aperture radar (SAR) images has received an increasing amount of attention from the image processing community [1-2]. Nevertheless, SAR images suffer from strong speckle multiplicative noise, which results in difficult image processing tasks. Among these processing tasks, segmentation is a key step for interpreting and understanding SAR images.

Recently, some variational frameworks based on curve evolution and level set methods (LSMs) have been proposed for SAR images segmentation. Germain and Refregier [3] proposed a snake-based segmentation model. We note that such parametric active contour scheme presents an evidential limitation, i.e., topological changes which occur during the evolution of the curve become difficult. In [4-6], the approaches based on the LSM are proposed for SAR images segmentation. Ayed et al. [4] designed a scheme to partition SAR images into multiple homogeneous regions, but it is difficult to set an appropriate criterion to terminate the curve evolution. Shuai and Sun [5] improved the method proposed in [4] by employing an efficient criterion for the front propagation convergence. Inspired by the image restoration model in the case of multiplicative noise, Le and Vese [6] introduced a piecewise constant segmentation model. Note here that these mentioned methods based on the traditional LSM can overcome the topological change difficulty in [3]. However, they may result in an unexpected state since the corresponding energy functional has a local minimum. Meanwhile, these methods consist of initializing the active contour in a distance function and re-initializing periodically during the evolution, which is time-consuming.

More recent, some new developments, such as the convex techniques [7-8] and some fast algorithms [9-10], have improved the segmentation in both efficiency and accuracy for optical images. Since the successes of those models are founded on the assumption that the images are corrupted by some additive Gaussian noises, they are not directly suitable for non-Gaussian noise problems.

In this paper, we present a fast and efficient multiphase fuzzy region competition model for SAR image segmentation. The proposed functional contains two terms: one term measures the conformity of the data to a Gamma distribution model. The other is of regularization to obtain segmentation boundaries. Due to the presence of speckle noise, the original edge indication function based on gradients failed in SAR image segmentation. We introduce an edge detector based on the ratio of exponentially weighted averages (ROEWA) operator [11] to replace the gradient-based indicator [9]. To improve the computational efficiency, a variable splitting technique is combined with the augmented Lagrangian method (ALM) to minimize the energy functional. The efficiency of the ALM has been demonstrated in [12-13].

The remainder of the paper is organized as follows. In Section II, some related works are reviewed. Section III presents our new segmentation model and discusses the proposed algorithm in detail. Numerical experimental results are given in Section IV to show the performance of our algorithm. Section V concludes the paper.

Corresponding author, Cunliang Liu

doi:10.4304/jsw.8.1.228-235

II. Related Works

A. Multiphase Fuzzy Region Competition Framework

Let $\Omega \in \mathbb{R}^2$ be the image domain, and $I(s): \Omega \to \mathbb{R}$ be a given image, where $s = (x, y)$ is a pixel in Ω. Potts [14] proposed a hard multiphase segmentation model, which aims to partition Ω into n sub-domains $\{\Omega_i\}_{i=1}^n$ by minimizing the following constrained energy

$$\begin{aligned} &\min_{\Omega_i}\{\gamma \sum_{i=1}^{n} \left|\partial\Omega_i\right| + \sum_{i=1}^{n} \int_{\Omega_i} Q_i(s)ds\} \\ &\text{s.t. } \Omega = \bigcup_{i=1}^{n} \Omega_i,\ \Omega_i \bigcap_{i \neq j} \Omega_j = \varnothing \end{aligned} \tag{1}$$

where the first term is called the regularization term, and the second is the fidelity term. γ is a tuning parameter to balance these two terms. The notation $|\partial\Omega_i|$ measures the length of the boundary of the sub-domain Ω_i. The function Q_i is defined to evaluate the performance of the label assignment at each partition Ω_i.

Pan et al. [15] proposed to use $n-1$ level set functions to represent n regions. Thus, the functional in (1) can be reformulated in terms of the level set function as follows

$$\min_{\phi_j}\{\gamma \sum_{j=1}^{n-1} \int_{\Omega} \left|\nabla H(\phi_j(s))\right| ds + \sum_{i=1}^{n} \int_{\Omega} Q_i(s)\psi_i(s)ds\} \tag{2}$$

where $\phi_j\,(j = 1, 2, ..., n-1)$ is the level set function, $\psi_i\,(i = 1, 2, ..., n)$ is the characteristic function of the region Ω_i, and $H(\cdot)$ is the Heaviside function. A more popular form of Q_i is $(I - c_i)^2$ where $c_i\,(i = 1, 2, ..., n)$ is the mean intensity value on Ω_i (see [15] for more details).

Mory et al. [8] introduced to use the fuzzy membership function to represent the region and minimize the two-phase fuzzy region competition energy. Following the idea of [8], we introduce the fuzzy membership function $u_j \in [0,1]$ to replace the level set function ϕ_j, and relax the multiphase segmentation model (2) into a soft form

$$\min_{0 \le u_j \le 1}\{\gamma \sum_{j=1}^{n-1} \int_{\Omega} \left|\nabla u_j(s)\right| ds + \sum_{i=1}^{n} \int_{\Omega} Q_i(s)\psi_i(s)ds\} \tag{3}$$

B. MAP Estimation and Gamma Distribution Model

Following [16-17], the partition $R(\Omega) = \{\Omega_i\}_{i=1}^n$ of the image domain can be computed via the maximum a-posteriori probability (MAP) estimation. An appropriate choice of probability densities is required to handle the different perturbation effects of noise models accurately. In the case of an L-look SAR image, Ω_i was modeled by a Gamma distribution as follows [4]

$$p_i(I(s)) = \frac{L^L}{c_i \Gamma(L)} \left(\frac{I(s)}{c_i}\right)^{L-1} e^{-\frac{LI(s)}{c_i}} \tag{4}$$

The image in each region Ω_i is therefore characterized by its mean c_i and the number of looks L. Using this noise model, the function Q_i is rewritten by the negative log-likelihood estimation

$$Q_i = -\log p_i(I) \simeq \ln I - L \ln LI + L \ln c_i + \frac{LI}{c_i} \tag{5}$$

where

$$c_i = \frac{\int_{\Omega} I\psi_i ds}{\int_{\Omega} \psi_i ds} \tag{6}$$

C. ROEWA-based Edge Detector

In the case of optical images, an edge is usually defined as a local maximum of the gradient magnitude in the gradient direction. The edge detection function is typically chosen as $g(|\nabla I|) = 1/(1 + |\nabla I|^2)$ in [9]. However, such image edge information based on gradients is not accurate if the image is corrupted by some multiplicative speckle noises [11].

In earlier works, several edge detectors were developed, e.g., based on a ratio of averages (ROA), or a generalized likelihood ratio (GLR). However, they are optimal only in the mono-edge case. Aiming at the drawback of the mono-edge model, Fjortoft et al. [11] put forward a multi-edge detector, which was the ROEWA operator. Let us give a brief introduce to this approach.

To estimate the local mean values under the stochastic multi-edge model and the multiplicative noise model, a linear minimum mean square error (MMSE) filter was introduced. The MMSE filter will be split along the vertical and horizontal axes, and the weighted means estimated in the different half windows will be used for edge detection.

To facilitate the implementation, we suppose the filter to have separable impulse response $f_{2D}(s) = f(x)f(y)$ and first consider the 1D case. In the discrete case, f can be implemented by means of a pair of recursive filters $f_1(w)$ and $f_2(w)$, realizing the normalized causal and anti-causal part of $f(w)$, respectively

$$\begin{cases} f_1(w) = ae_1(w) + bf_1(w-1) & w = 1, 2, ..., N \\ f_2(w) = ae_2(w) + bf_2(w+1) & w = N, N-1, ..., 1 \end{cases} \tag{7}$$

where $b = e^{-a}$, $a = 1 - b$, w is the spatial index, and $e_1(w)$ and $e_2(w)$ are the inputs of $f_1(w)$ and $f_2(w)$, respectively. The smoothing function f can be written as

$$f(w) = \frac{1}{1+b} f_1(w) + \frac{b}{1+b} f_2(w-1) \tag{8}$$

The exponentially weighted averages $\hat{\mu}_1$ and $\hat{\mu}_2$ are normalized to be unbiased deviation, so we can normalize the ratio to be superior to one

$$r_{\max} = \max\{\frac{\hat{\mu}_1}{\hat{\mu}_2}, \frac{\hat{\mu}_2}{\hat{\mu}_1}\} \tag{9}$$

The image $I(x, y)$ is first smoothed column by column using the 1D smoothing filters to compute the horizontal edge strength component. Next, the causal and anti-causal filters f_1 and f_2 are employed line by line on the result of smoothing operation to obtain $\hat{\mu}_{X1}$ and $\hat{\mu}_{X2}$

$$\begin{cases}\hat{\mu}_{X1}(x,y) = f_1(x) * (f(y) \bullet I(x,y)) \\ \hat{\mu}_{X2}(x,y) = f_2(x) * (f(y) \bullet I(x,y))\end{cases} \tag{10}$$

Here $*$ denotes convolution in the horizontal direction and $\bullet$ denotes convolution in the vertical direction. The normalized ratio $r_{X\max}$ is found by substituting $\hat{\mu}_{X1}$ and $\hat{\mu}_{X2}$ into (9). The vertical edge strength component $r_{Y\max}$ is obtained in the same manner, except that the directions are interchanged.

With analogy to gradient based edge detectors for optical images, we take the magnitude of the two components

$$|r_{2D\max}(x,y)| = \sqrt{r_{X\max}^2(x,y) + r_{Y\max}^2(x,y)} \tag{11}$$

Finally, we substitute $|r_{2D\max}(x,y)|$ into g and get the following new edge detector

$$g_r(|r_{2D\max}|) = \frac{1}{1+|r_{2D\max}(x,y)|^2} \tag{12}$$

III. The Proposed Method

In this section, we shall present and discuss the details of our proposed improved SAR image segmentation model and its numerical implementation.

A. *The Proposed Energy Functional*

By inserting the new edge detector (12) and the negative log-likelihood estimation (5), as well as the multiphase fuzzy region competition framework (3), we finally minimize the following energy functional

$$\min_{0\le u_j\le 1}\{\gamma\sum_{j=1}^{n-1}\int_\Omega g_r\left|\nabla u_j(s)\right|ds + \sum_{i=1}^{n}\int_\Omega Q_i(s)\psi_i(s)ds\} \tag{13}$$

B. *Fast Minimization Based on the ALM*

A typical numerical scheme for multiphase image segmentation is the gradient descent method, which is actually very slow [15]. The reason is that the discrete numerical approximation for the total variation term requires a numerical smoothing parameter to avoid numerical instabilities. It would prevent the resulting algorithm from converging to the true optimizer.

For the purpose of efficiency, we follow the idea in [12-13] and take use of the ALM, which is a combination of the multiplier method and the penalization method. They share the similarity of converting a constrained optimizing problem into an unconstrained one.

For that end, we add auxiliary variables $\vec{d}_j$ by using the variable splitting technique and approximate (13) by

$$\min_{0\le u_j\le 1}\{\gamma\sum_{j=1}^{n-1}\int_\Omega g_r\left|\vec{d}_j\right|ds + \sum_{i=1}^{n}\int_\Omega Q_i\psi_i ds\} \text{ s.t. } \vec{d}_j = \nabla u_j \tag{14}$$

By doing this, the minimization of (14) becomes a constrained optimizing problem, which can be solved with the ALM. Define $K_j = \vec{d}_j - \nabla u_j$ under the constraint $\vec{d}_j = \nabla u_j$, this then leads to the following unconstraint problem

$$\begin{gathered}\min_{0\le u_j\le 1}\{\gamma\sum_{j=1}^{n-1}\int_\Omega g_r\left|\vec{d}_j\right|ds + \sum_{i=1}^{n}\int_\Omega Q_i\psi_i ds + \\ \sum_{j=1}^{n-1}\int_\Omega \lambda_j K_j ds + \frac{\theta}{2}\sum_{j=1}^{n-1}\int_\Omega K_j^2 ds\}\end{gathered} \tag{15}$$

In the above, λ_j is called the Lagrange multiplier, and θ is a penalization parameter. Because energy (15) is a minimization problem with multiple variables, the minimization procedure can be decomposed into the following iteratively solved sub-problems

$$\begin{cases} u_j^{k+1} = \arg\min_{0\le u_j\le 1}\{\sum_{i=1}^{n}\int_\Omega Q_i\psi_i ds + \int_\Omega \lambda_j K_j ds + \frac{\theta}{2}\int_\Omega K_j^2 ds\} \\ \vec{d}_j^{k+1} = \arg\min_{\vec{d}_j}\{\gamma\int_\Omega g_r\,|\vec{d}_j|\,ds + \int_\Omega \lambda_j K_j ds + \frac{\theta}{2}\int_\Omega K_j^2 ds\} \\ \lambda_j^{k+1} = \lambda_j^k + \theta K_j(u_j^{k+1}) \end{cases} \tag{16}$$

The first sub-problem of u_j^{k+1} can be obtained by taking the following Euler-Lagrange equation

$$\sum_{i=1}^{n} Q_i\frac{\partial\psi_i}{\partial u_j} - \theta\,\mathrm{div}\left(\nabla u_j - \vec{d}_j^{\,k}\right) = 0 \tag{17}$$

A fast solution of u_j^{k+1} is provided by a Gauss-Seidel iterative scheme. To ensure $u_j^{k+1}\in[0,1]$, we use the projection formula $u_j^{k+1} = \max\{\min\{u_j^{k+1},1\},0\}$.

For the second sub-problem, the closed form solution can be obtained by using the shrinkage operator [10]

$$\vec{d}_j^{k+1} = \max\left\{\left|\nabla u_j^k - \lambda_j^k/\theta\right| - g_r\,\gamma/\theta, 0\right\}\frac{\nabla u_j^k - \lambda_j^k/\theta}{\left|\nabla u_j^k - \lambda_j^k/\theta\right|} \tag{18}$$

At last, the third sub-problem is computed directly.

C. *Algorithm Details*

The proposed algorithm for multiphase SAR image segmentation is as follows (Algorithm I).

1. **Initialization**: $u_j^0, \lambda_j^0, \vec{d}_j^0$ and set $k=0$, for $i = 1,2,\ldots,n,\ j = 1,2,\ldots,n-1$.
2. **Repeat**
3. Update each c_i^{k+1} by (6);
4. Compute each u_j^{k+1} by (17);
5. Compute each $\vec{d}_j^{k+1}$ by (18);
6. $\lambda_j^{k+1} = \lambda_j^k + \mu K_j(u_j^{k+1})$;
7. $u_j^{k+1} = \max\{\min\{u_j^{k+1},1\},0\}$;
8. $k = k+1$;
9. **Until** a stopping criterion is satisfied.

IV. Experimental Results and Analysis

In this section, we demonstrate the proposed method on both synthetic and real SAR images. In our implementation, all the experiments are performed using MATLAB v7.0 on a Windows XP platform with an Intel Core 2 Duo CPU at 2.80 GHz and 2GB memory. To set up a relatively neutral criterion for comparison, we used the same initial contour for all the methods in each experiment. Moreover, we generally choose some parameters as follows: $u_j^0 = 0$, $\lambda_j^0 = 0$ and $\vec{d}_j^0 = 0$. The meter γ and θ is required to be tuned for each image. For the stopping criterion, we follow the approach in [18] and set the parameters $T_{it} = 10$ and $\xi_{length} = 5$.

A. Simulated Data

First, we adopt the following experiment to verify the validity of the new edge detector based on the ROEWA operator. This is done by replacing the ROEWA-based indicator with the gradient-based detector in the proposed approach. Figs. 1(a), (d) and (g) are three test images corrupted by multiplicative speckle noise with variance of 0.05, 0.2 and 0.5, respectively. Each image has four different regions ($n = 4$) and its size is 256×256 pixels. The final segmentation results for the gradient-based indicator are shown in Figs. 1(b), (e) and (h). We can observe that the gradient-based detector gives accurate edge when the noise in the image is weak, but in vain when the noisy is strong. However, as shown in Figs. 1(c), (f) and (i), the segmentation results based on the ROEWA operator could give the correct boundary of the region for all cases, with the weak edge location being more accurate especially. This is because the ROEWA-based term in the energy function could give a greater penalty to weak edges, and thus maintaining the edge information well and enhancing the segmentation accuracy.

We also give the segmentation accuracy with different detectors in Fig. 1. The accuracy of segmentation is analyzed by the error ratio (denoted as ER) in [19]. The comparison results show that the ROEWA-based approach is more flexible than the gradient-based one to cope with images with different degree of roughness.

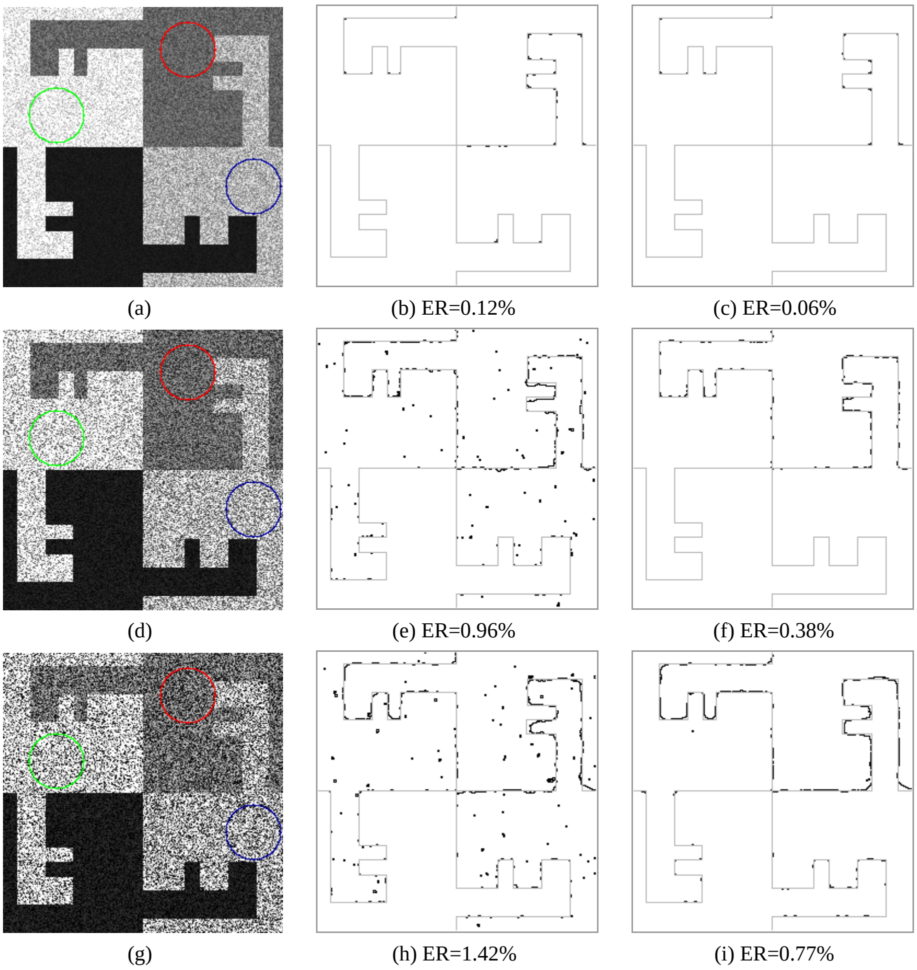

(a) (b) ER=0.12% (c) ER=0.06%

(d) (e) ER=0.96% (f) ER=0.38%

(g) (h) ER=1.42% (i) ER=0.77%

Figure 1. Edges detected by the gradient-based detector and ROEWA-based indicator, respectively. The First column: test images with initial contours; The Second column: segmentation results with gradient-based detector; The Third column: segmentation results with ROEWA-based indicator.

B. Real Data

We next test the proposed approach on various real SAR images. The prior knowledge about the real SAR images is shown in Table I. Fig. 2 shows the segmentation results with the method in [6], the method in [4] and the proposed method, respectively.

TABLE I
THE PRIOR KNOWLEDGE OF THE REAL SAR IMAGES

Image	Size (pixels)	Class	Band	Polarization	Image Source
Fig. 2(a)	100×182	2	X	HH	A domestic airborne radar image data
Fig. 2(e)	197×197	3	X	HH	Sandia National Laboratories
Fig. 2(i)	254×254	4	X	HH	DLR and EADS Astrium Company

In Fig. 2(a), a domestic airborne radar SAR imaging data is used to test the algorithm and the resolution is less than 1 m. The results demonstrate that the target in Fig. 2(d) is detected without false alarm by using the proposed model. But using the other two models, many pixels with brighter gray level are segmented to be target pixel in Figs. 2(b) and (c). It is clearly shows that the proposed method is more suitable for segmentation high-resolution SAR images.

An agricultural dataset is tested in Fig. 2(e). As we can see, this result in Fig. 2(f) is not satisfactory because there are a large number of false alarms in each region due to the speckle noise. Since the method doesn't consider the trait of multiplicative noise, it is not fit for multiplicative noise very well. Compared to Fig. 2(f), the speckle noise in Fig. 2(g) is significantly reduced, and the edges of the region are smoother. The reason is that the Gamma distribution fits the character of SAR images well. Compared to Fig. 2(g), the numbers of false alarms in Fig. 2(h) drop almost zero. This is because that the ROEWA-based term in the proposed energy functional can maintain the local edge information well, especially the weak edge information, which reduces the misclassification ratio.

In Fig. 2(i), we can also find that our method has a good performance of removing false alarms and suppressing speckle.

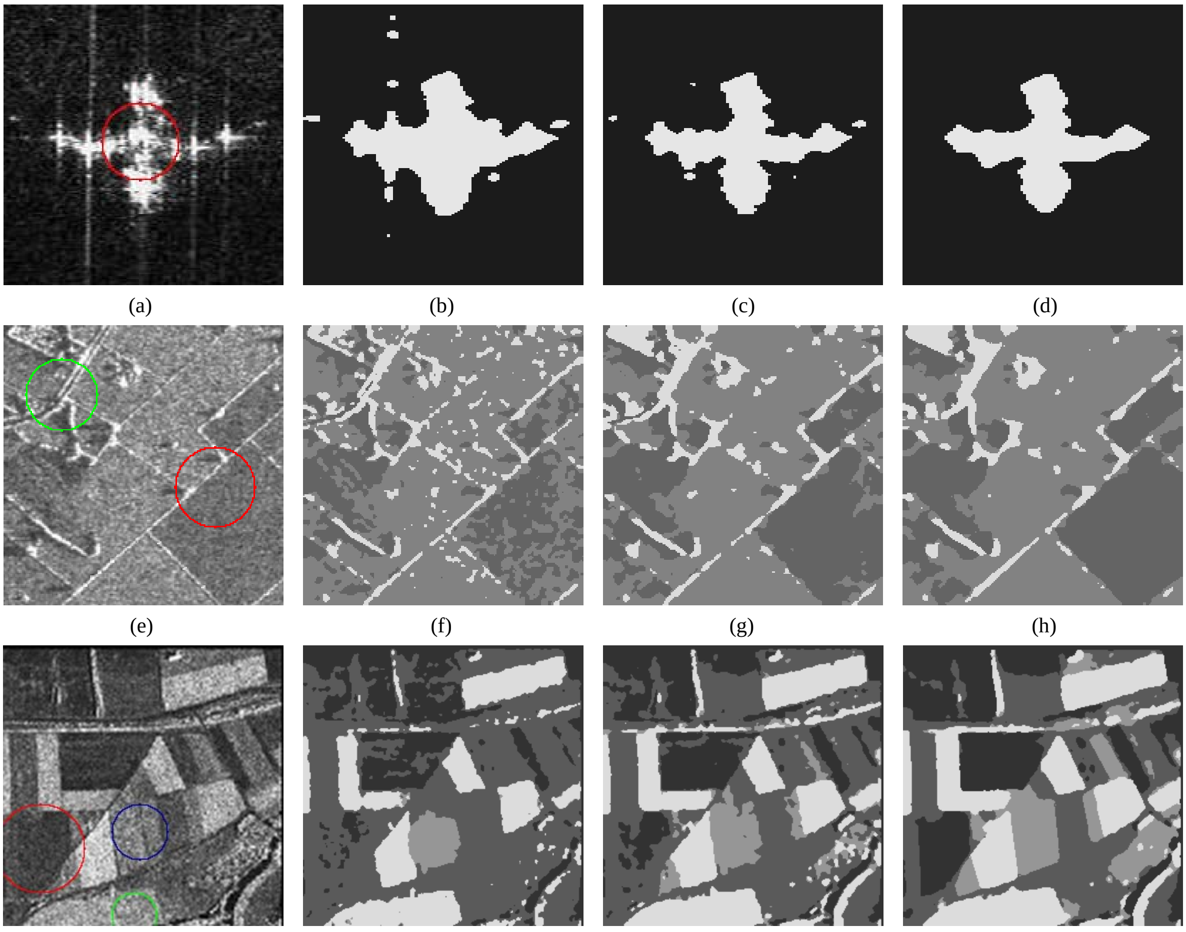

Figure 2. Segmentation results of three real SAR images. The first column: real SAR images with initialization segmentation; The second column: segmentation results by the method in [6]; The third column: segmentation results by the method in [4]; The fourth column: segmentation results by the proposed method.

The subjective evaluation of the segmentation results is given above, the objective evaluation criteria is as follows: the objective evaluation criteria contains three criteria: the variance RI_{var}, the mean RI_{mean} and the logarithm of the normalized likelihood ratio D of the ratio image [20]. RI_{var} describes the change of the pixel value in the ratio image. The smaller the value of RI_{var} is, the better the performance of segmentation algorithm is. RI_{mean} describes the situation of the suppression to speckle noise, and the closer the value of RI_{mean} approaches 1, the better the suppression to speckle noise is. D is allowed to be the value around zero. And only when all pixels have the same intensity, it gets zeros. The smaller the value of $|D|$ is, the better the performance is. As shown in Table II, the proposed algorithm achieves better performance according to the three criteria of ratio image. The subjective evaluation consists with the objective evaluation, which fully indicated the effectiveness and the universality of our proposed algorithm.

TABLE II
COMPARISON OF SEGMENTATION PERFORMANCE USING DIFFERENT SEGMENTATION METHODS

Image	Method in [6]			Method in [4]			The proposed method		
	$\|D\|$	RI_{mean}	RI_{var}	$\|D\|$	RI_{mean}	RI_{var}	$\|D\|$	RI_{mean}	RI_{var}
Fig. 2(a)	0.1629	1.0213	0.3417	0.1580	1.0127	0.3143	0.1533	1.0105	0.2951
Fig. 2(e)	0.0140	1.0374	0.0269	0.0125	1.0231	0.0243	0.0101	1.0090	0.0206
Fig. 2(i)	0.0693	1.0448	0.0868	0.0631	1.0276	0.0682	0.0584	1.0107	0.0623

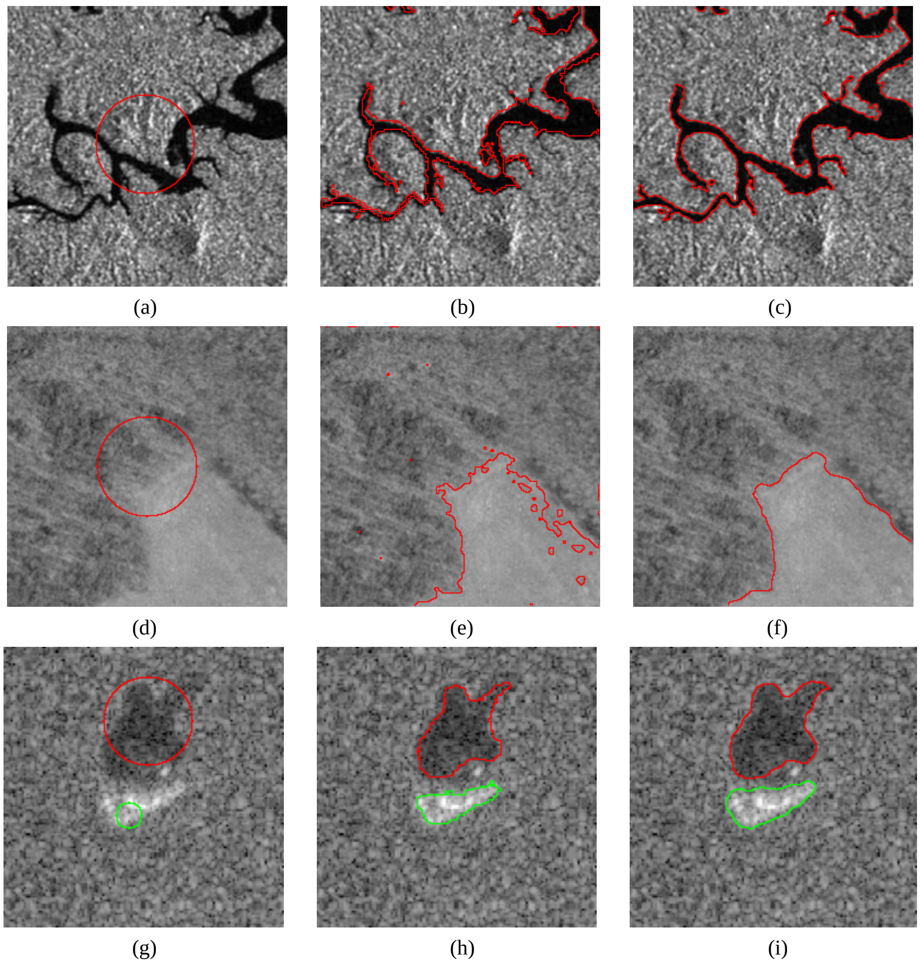

Figure 3. Comparison of segmentation results with the proposed method and some other typical methods. The first column: initial segmentation; (b) and (e) Segmentation result by the method in [21]; (h) Segmentation result by the method in [22]; The Third column: segmentation results by the proposed method.

In Fig. 3, we make comparison our method with some other typical segmentation methods for SAR image. Figs. 3(a) and (d) are tested in [21]. The segmentation results by the multi-scale probability neural network method in [21] are shown in Figs. 3(b) and (e). Our method gives more satisfactory results in Fig. 3(c) since the small branches of river are better segmented while in Fig. 3(b) many branches are broken. Also, our result in Fig. 3(f) has a smooth boundary and is more accurate than that in Fig. 3(e). Fig. 3(g) shows a real MSTSAR SAR image of vehicle T72 which has been tested in [22]. This image contains three regions: target, shadow and background. Fig. 3(i) shows the three-phase segmentation result of our proposed method. Our result is competitive with the result in Fig. 3(h) by method in [22].

At last, to show the computational efficiency of the proposed approach compared to the level set based SAR image segmentation approaches in [6,4]. The number of iterations and the time consuming that needed for the algorithm convergence of each method are shown in Table III. It is shown that the proposed method needs less iterations and computational time compared to the other two methods. This justifies the using of the ALM for energy minimization.

TABLE III
COMPARISON OF ITERATIONS AND COMPUTATION TIME USING DIFFERENT SEGMENTATION METHODS

Image	Method in [6]		Method in [4]		The proposed method	
	Iterations	Time (s)	Iterations	Time (s)	Iterations	Time (s)
Fig. 2(a)	535	6.414	459	5.227	117	1.472
Fig. 2(e)	550	42.983	506	30.031	130	7.963
Fig. 2(i)	617	149.718	594	116.483	159	22.387

V. CONCLUSIONS

A general multiphase fuzzy region competition model for SAR image segmentation is proposed in this paper. There are two novelties. One is that a fuzzy membership function is introduced to represent the region for handling multiphase segmentation. The other is the ROEWA-based edge detector is incorporated into the new energy functional. Furthermore, the proposed method is faster and easier to implement than the other curve evolution based methods. According to our experimental results, we find that our approach is competitive with other state-of-the-art segmentation methods for SAR images.

ACKNOWLEDGMENT

This work was supported in part by National Natural Science Funds of China (No. 61170106), and Natural Science Foundation of Shandong Province (No. ZR2010FQ030).

REFERENCES

[1] H. Zhang, Z. Duan, Z. Zhu, Y. Wang, “Fast moving object segmentation based on active contours,” Journal of Computers, 2012, vol. 7, no. 4, pp. 863-869.

[2] Z. Ye, Z. Hu, X. Lai, H. Chen, “Image segmentation using thresholding and swarm intelligence,” Journal of Software, 2012, vol. 7, no. 5, pp. 1074-1082.

[3] O. Germain and P. Refregier, “Edge location in SAR images: Performance of the likelihood ratio filter and accuracy improvement with an active contour approach,” IEEE Transactions on Image Processing, 2001, vol. 10, no. 1, pp. 72-78.

[4] I. B. Ayed, A. Mitiche, and Z. Belhadj, “Multiregion level-set partitioning of synthetic aperture radar images,” IEEE Transactions on Pattern Analysis and Machine Intelligence, 2005, vol. 27, no. 5, pp. 793-800.

[5] Y. Shuai and H. Sun, “SAR image segmentation based on level set with stationary global minimum,” IEEE Transactions on Geoscience and Remote Sensing Letters, 2008, vol. 5, no. 4, pp. 644-648.

[6] M. Le and A. Vese, “Additive & multiplicative piecewise-smooth segmentation models in a functional minimization approach,” Interpolation Theory and Applications: A conference in honor of Michael Cwikel, Miami, Florida, Editors: Laura De Carli and Mario Milman, Comtemporay Mathematics, 2007, vol. 445, pp. 207-223.

[7] T. F. Chan, S. Esedoglu, and M. Nikolova, “Algorithms for finding global minimizers of image segmentation and denoising models,” SIAM Journal on Applied Mathematics, 2006, vol. 66, no. 5, pp. 1632-1648.

[8] B. Mory and R. Ardon, “Fuzzy region competition: a convex two-phase segmentation framework,” SSVM 2007, LNCS 4485, pp. 214-226, 2007.

[9] X. Bresson, S. Esedoglu, P. Vandergheynst, J.-P. Thiran, and S. Osher, “Fast global minimization of the active contour/snake model,” Journal of Mathematical Imaging and Vision, 2007, vol. 28, no. 2, pp. 151-167.

[10] T. Goldstein, X. Bresson, and S. Osher, “Geometric applications of the Split Bregman method: segmentation and surface reconstruction,” Journal of Scientific Computing, 2010, vol. 45, no. 1, pp. 272-293.

[11] R. Fjortoft, A. Lopes, and P. Marthon, “An optimal multiedge detector for SAR image segmentation,” IEEE Transactions on Geoscience and Remote Sensing, 1998, vol. 36, no. 3, pp. 793-802.

[12] C. Wu and X.-C. Tai, “Augmented Lagrangian method, dual methods, and Split Bregman iteration for ROF, vectorial TV, and high order models,” SIAM Journal on Imaging Sciences, 2010, vol. 3, pp. 300-339.

[13] M. V. Afonso, J. M. Bioucas-Dias, and M. A. T. Figueiredo, “An augmented lagrangian approach to the constrained optimization formulation of imaging inverse problems,” IEEE Transactions on Image Processing, 2011, vol. 20, no. 3, pp. 681-695.

[14] R. B. Potts, “Some generalized order-disorder transformations,” Mathematical Proceedings of the Cambridge Philosophical Society, 1952, vol. 48, no. 1, pp. 106-109.

[15] Z. Pan, H. Li, W. Wei, Z. Guo, and C. Zhang, “A variational level set method of multiphase segmentation for 3D images,” Chinese Journal of Computers, 2009, vol. 32, no. 12, pp. 2464-2474.

[16] S. C. Zhu and A. Yuille, “Region competition: Unifying snakes, region growing, and bayes/mdl for multiband image segmentation,” IEEE Transactions on Pattern

Analysis and Machine Intelligence, 1996, vol. 18, pp. 884-900.
[17] N. Paragois and R. Deriche, “Geodesic active regions: A new paradigm to deal with frame partition problems in computer vision,” Journal of Visual Communication and Image Representation, 2002, vol. 13, pp. 249-268.
[18] X. Wang, D. Huang, and H. Xu, “An efficient local Chan-Vese model for image segmentation,” Pattern Recognition, 2010, vol. 43, pp. 603–618.
[19] S. Han, W. Tao, and X. Wu, “Texture segmentation using independent-scale component-wise Riemannian-covariance Gaussian mixture model in KL measure based multi-scale nonlinear structure tensor space,” Pattern Recognition, 2011, vol. 44, no. 3, pp. 503-518.
[20] R. Caves, S. Quegna, and R. White, “Quantitative comparison of the performance of SAR segmentation algorithms,” IEEE Transactions on Image Processing, 1998, vol. 17, no. 11, pp. 1534-1546.
[21] J. Quan, X. Wen, and X. Xu, “Multiscale probabilistic neural network method for SAR image segmentation,” Applied Mathematics and Computation, 2008, vol. 205 pp. 578-583.
[22] G. Gao, L. Zhao, J. Zhang, D. Zhou and J. Huang, “A segmentation algorithm for SAR images based on the anisotropic heat diffusion equation,” Pattern Recognition, 2008, vol. 41, pp. 3035-3043.

Cunliang Liu was born in 1977. He received the B.S. degree and M.S. degree in computer application technology from the Shenyang Ligong University, Shenyang, China, in 2000 and 2003, respectively. He is currently a lecturer in the College of Information Engineering at Qingdao University. His research interests include image segmentation, the variational methods and PDEs in image processing.

Yongguo Zheng was born in 1963. He is currently a Professor of computer science at Shandong University of Science & Technology. Zheng’s research interests lie in the area of computer vision, image segmentation, object recognition, and tracking.

Zhenkuan Pan was born in 1966. He received his Ph.D. degree in engineering mechanics from Shanghai Jiao Tong University, China in 1992. Currently he is a professor of the College of Information Engineering at Qingdao University. His research interests include dynamics and control of multibody systems, computer simulation and variational image processing. He has published numerous papers and conference papers in the area of image processing and object recognition.

Jinming Duan was born in 1989. Currently he is a postgraduate student of the College of Information Engineering at Qingdao University. His research interests include variational image processing, and three-dimensional reconstruction.

Guodong Wang was born in 1980. He received his Ph.D degree in the Institute for Pattern Recognition and Artificial Intelligence, Huazhong University of Science and Technology, China in 2008. Currently he is a lecturer of the College of Information Engineering at Qingdao University. His research interests include image analysis and variational image processing.